Open Applied Science

https://openappscience.science

Resilient Feeder Restoration through Risk-Aware Grid Decision Modeling: Reliable Recovery from Sparse Sensor Evidence during Extreme Weather across Energy Infrastructures

Alessia Piras, Stefano L. Ferrari, Andrea Santoro

Department of Electrical, Electronic and Information Engineering, School of Engineering and Architecture, University of Bologna, Bologna, Emilia-Romagna, Italy

Abstract

This paper presents a comprehensive risk-aware grid decision modeling framework designed to achieve reliable feeder recovery using sparse, heterogeneous, and asynchronous sensor evidence during extreme weather events. By fusing surviving supervisory control and data acquisition measurements, micro-phasor telemetry, smart meter last-gasp notifications, and meteorological fragility priors, the framework generates calibrated probability distributions of unobserved line statuses and post-outage cold load pickup demands. These probabilistic beliefs directly inform a sequential switching and distributed resource dispatch model that explicitly constrains tail-risk operational violations across coupled electrical, natural gas, and district heating infrastructures. Extensive numerical validations on modified multi-energy benchmark feeders demonstrate that the proposed methodology significantly enhances load recovery reliability, eliminates protective relay misoperations, and outperforms conventional restoration paradigms under severe telemetry attrition.

Keywords: Feeder restoration, risk-aware decision modeling, sparse sensor observability, extreme weather resilience

1. Introduction

1.1 Impact of Extreme Weather on Modern Energy Infrastructures

The accelerating frequency and intensity of extreme weather phenomena, including major hurricanes, severe ice storms, atmospheric rivers, and catastrophic wildfires, pose unprecedented challenges to the structural integrity and operational continuity of modern energy infrastructures. Consequently, over eighty percent of customer power interruptions during severe meteorological events originate within the distribution domain. When a high-intensity meteorological front traverses a regional distribution network, it rarely causes isolated, single-component contingencies [1].

Furthermore, contemporary energy distribution is no longer confined to isolated electrical networks. The rapid proliferation of gas-fired distributed generation, combined heat and power plants, electric heat pumps, and electrified water distribution pumping stations has created deeply interdependent multi-energy infrastructures. Therefore, achieving resilient feeder restoration requires a holistic operational paradigm that accounts for both the physical vulnerabilities of electrical distribution components and the cross-sector interdependencies binding modern energy infrastructures together. Power-network frequency-control reviews provide context for the control layer beneath restoration decisions [2].

1.2 The Observability Crisis and Sparse Sensor Evidence

A critical yet frequently overlooked dimension of extreme weather resilience is the vulnerability of the cyber-physical telemetry and communication layer that underpins modern distribution management systems. However, extreme weather events simultaneously assault both the physical power delivery apparatus and

the supporting communication infrastructure. Cellular base stations lose backup power, fiber-optic backhaul cables affixed to utility poles are severed by falling timber, and localized radio-frequency mesh networks suffer severe signal attenuation due to torrential precipitation and physical debris [3]. A separate research setting concerns integrated management of spacecraft tests [4].

This concurrent degradation of the cyber-telemetry layer precipitates an acute observability crisis precisely when situational awareness is most urgently needed. Distribution system operators are left to navigate complex restoration procedures using sparse, fragmented, and asynchronous sensor evidence. In many field scenarios, up to seventy or eighty percent of remote terminal units and smart meters within an impacted service territory may become unresponsive or transmit corrupted, time-delayed data packets. This context also permits comparison with cybersecurity of connected urban energy systems [5]. A separate research setting concerns temperature compensation in resistive hydrogen sensing [6].

1.3 Research Objectives and Structural Organization

Rather than treating state estimation and service restoration as decoupled, sequential processes where point estimates of network topology are fed into deterministic optimization engines, decision models must internalize the epistemic and aleatory uncertainties arising from sparse sensor evidence. The primary objective of this research is to establish a unified, risk-aware grid decision modeling framework capable of orchestrating reliable, multi-step feeder recovery across coupled energy infrastructures despite pervasive sensor loss during extreme weather events. An application-specific perspective concerns fiber-optic current sensing with continuous illumination [7].

To accomplish this overarching objective, this study develops a two-pillar methodological architecture. The first pillar consists of a physics-informed, spatio-temporal evidence reconstruction mechanism that synthesizes surviving electrical measurements, asynchronous equipment status flags, and meteorological fragility curves to infer posterior probability distributions over unobserved fault locations and post-outage load demands [8]. The second pillar translates these probabilistic state beliefs into a multi-stage, risk-averse sequential decision model that coordinates feeder sectionalizing, tie-switch closures, distributed energy resource dispatch, and cross-energy conversion while strictly bounding the conditional tail risk of thermal overloads, voltage collapse, and protective relay trip events [9].

2. Literature Review and Theoretical Background

2.1 Evolution of Distribution System Service Restoration

Early methodologies relied predominantly on pre-compiled heuristic rules, expert systems, and fuzzy logic inference engines designed to mimic the operational reasoning of human dispatchers. While these rule-based frameworks offered rapid execution times suitable for early-generation control centers, they lacked mathematical guarantees of optimality and frequently failed to identify feasible switching sequences when confronted with complex, multi-fault contingencies that fell outside pre-programmed operational scenarios. Related methodological comparisons include cooperative atomic sites for fuel-cell electroreduction [10]. Optimized fractional-order control has also been studied in interconnected multi-source power systems [11].

2.2 State Estimation and Fault Localization under Low Observability

Traditional weighted least squares state estimation algorithms require topological redundancy of measurements to filter sensor noise and detect bad data, a condition rarely satisfied in radial distribution feeders without extensive pseudo-measurement generation [12]. During extreme weather events, the loss of communication channels and field sensors exacerbates this observability deficit, rendering conventional algebraic state estimators mathematically unsolvable due to rank deficiency in the measurement Jacobian matrix [13].

2.3 Risk-Averse Optimization in Coupled Energy Networks

Two-stage and multi-stage stochastic programming frameworks model uncertain parameters—such as renewable generation output, load fluctuations, and random component failures—through discrete scenario trees, optimizing the expected value of system recovery metrics across all postulated realizations. However,

optimizing purely for expected performance is fundamentally inadequate during extreme weather emergencies. Expected-value optimization is risk-neutral; it permits severe, potentially catastrophic operational violations in low-probability scenarios provided those losses are offset by high performance in more probable scenarios. A separate research setting concerns feature selection in fuzzy-rule networks [14]. A separate research setting concerns reinforcement-based switching of vehicle communication channels [15].

3. Sparse Sensor Evidence Reconstruction and Observability Modeling

3.1 Multi-Modal Telemetry Aggregation and Evidence Fusion

To establish a coherent foundation for decision modeling, the proposed framework implements a multi-modal telemetry aggregation and evidence fusion layer that systematically categorizes and processes all surviving information streams. Rather than discarding incomplete data packets or waiting for synchronous polling cycles that may never complete, the ingestion engine treats every incoming signal as a discrete piece of probabilistic evidence regarding the true latent state of the physical infrastructure. A separate research setting concerns public expenditure and sustainable development [16].

The surviving telemetry is classified into four distinct evidentiary modalities. The first modality comprises continuous, high-precision electrical measurements obtained from substation breaker instrumentation and surviving micro-phasor measurement units deployed at strategic feeder junctions. In degraded communication environments, these devices may fail to report their current state or may transmit delayed lock-out flags triggered by transient overcurrent events rather than permanent physical conductor failure.

The third modality consists of asynchronous, event-driven notifications generated by edge devices, primarily advanced metering infrastructure last-gasp signals and automated pressure or temperature alarms from coupled natural gas regulator stations and district heating heat exchangers. Because smart meters rely on fragile local mesh networks and limited capacitor energy reserves to transmit outage notifications upon power loss, the reception of a last-gasp signal confirms de-energization, whereas the absence of a signal is ambiguous, potentially indicating either continued energization or communication packet collision. An application-specific perspective concerns automated blood-pressure control in critical care [17].

Table 1: Characteristics and Failure Modes of Multi-Modal Grid Telemetry During Extreme Weather

Telemetry Modality	Primary Measurement Variables	Typical Reporting Latency	Primary Extreme Weather Failure Mechanism	Evidentiary Reliability Under Sparsity
Substation SCADA	Bus voltage, feeder root current, breaker status	2 to 4 seconds	Substation flooding, backhaul fiber severance	Very High for root node, low spatial granularity
Micro-Phasor Units	Synchrophasor voltage and current, frequency	20 to 100 milliseconds	GPS antenna damage, cellular tower outage	High precision, enables impedance triangulation
Field Reclosers and FCI	Switch open/close state, fault passage flags	5 to 30 seconds	Pole collapse, battery exhaustion, RTU damage	Moderate, prone to false positives from transients
Smart Meter AMI	Last-gasp outage flag, voltage sag logs	1 to 15 minutes	RF mesh congestion, meter destruction, packet drop	Asymmetric, high confidence on receipt, ambiguous on silence
Coupled Energy Sensors	Gas pipeline pressure, thermal loop flow rate	30 to 120 seconds	Telemetry power loss, pneumatic line freezing	High cross-sector correlation value for load inference

3.2 Probabilistic Topology Identification from Degraded Signals

To translate the aggregated multi-modal evidence into actionable topological intelligence, the distribution network and its coupled energy subsystems are modeled as a directed probabilistic graphical model, specifically a dynamic hybrid Bayesian network whose structural topology mirrors the physical connectivity of the feeders. In this graphical representation, each physical line segment, transformer, switch, and coupled energy converter is assigned a latent discrete state variable representing its true operational condition (intact, permanently faulted, or temporarily locked out) alongside continuous latent variables representing local nodal voltages and phase power injections.

When an extreme weather front impacts the network, the baseline prior probabilities of the latent component states are first initialized using the spatio-temporal meteorological fragility module described in the subsequent subsection [18] [19]. For instance, if a surviving micro-phasor unit located three miles downstream of a substation records zero voltage, and an automated recloser one mile upstream of that unit fails to communicate, the inference engine combines the downstream zero-voltage evidence with the substation breaker current reading to update the posterior probability that the silent recloser has tripped open due to a fault located between the two points.

Furthermore, the evidence reconstruction engine explicitly accounts for the asymmetric nature of communication failures. By modeling the communication network topology alongside the physical power grid, the algorithm distinguishes between independent random packet drops and correlated communication blackouts caused by the loss of a shared cellular base station or fiber aggregation node [20] [21]. The output of this probabilistic topology identification stage is not a single deterministic network graph, but rather a calibrated joint probability distribution over the set of plausible post-contingency network topologies, accompanied by marginal fault probabilities for every individual line segment lacking direct telemetry.

3.3 Spatio-Temporal Weather Fragility Integration

In regions of the feeder where communication loss is total and no electrical measurements can propagate due to upstream open switches, purely data-driven state estimation becomes completely uninformative. To prevent the decision model from operating blindly in these dark zones, the framework integrates physics-based spatio-temporal weather fragility models directly into the prior probability synthesis layer. Extreme weather events exhibit strong spatial correlation and predictable temporal progression as meteorological fronts move across a geographical service territory [22]. By tracking the real-time trajectory of wind gusts, ice accretion thickness, or floodwater elevation across a high-resolution geographic information system grid, the framework evaluates the localized mechanical stress imposed on every physical asset [23].

Each overhead conductor span, utility pole, and pad-mounted component is characterized by a structural fragility curve that maps environmental intensity measures to the conditional probability of structural failure [24]. Rather than relying on generic, homogeneous fragility curves, the model adjusts asset vulnerability dynamically based on local structural modifiers, including pole material and age, conductor cross-sectional area, span length, soil saturation levels affecting foundation stability, and surrounding LiDAR-derived tree canopy height and species profiles.

Beyond structural damage assessment, the weather fragility module also constructs probabilistic estimates of post-outage cold load pickup demand and distributed generation availability within unmonitored zones. By correlating outage duration tracking with external ambient temperature trajectories and building thermal envelope models, the reconstruction engine generates probabilistic envelopes of expected restoration load profiles for every de-energized load block, ensuring that subsequent switching decisions do not inadvertently trigger thermal overloads upon re-energization [25].

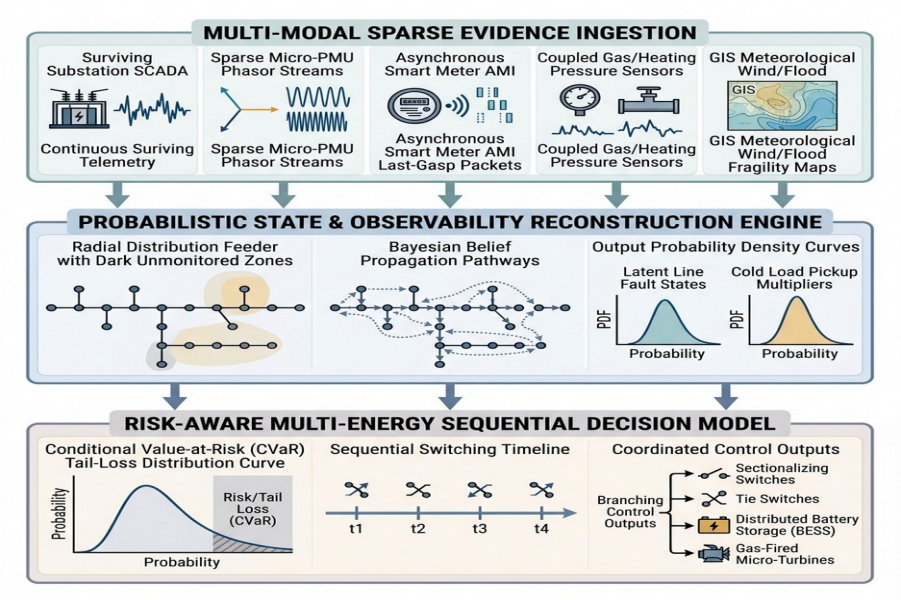


Figure 1: Comprehensive Architecture of the Spatio-Temporal Evidence Reconstruction and Risk-Aware Feeder Restoration Framework

4. Risk-Aware Grid Decision Modeling for Feeder Restoration

4.1 Conditional Value-at-Risk Formulation in Descriptive Terms

Because the underlying network topology and load magnitudes remain uncertain, any switching action carries an inherent operational risk. To manage this risk systematically, the restoration problem is formulated as a multi-stage, risk-averse mixed-integer optimization model governed by the Conditional Value-at-Risk metric.

In descriptive analytical terms, the decision model seeks to maximize an objective function composed of two primary competing components weighted by an operator-specified risk-aversion parameter. The second component penalizes the Conditional Value-at-Risk of operational loss across the ensemble of probabilistic topology and load scenarios generated by the evidence reconstruction engine [26].

For any candidate switching sequence, a threshold loss value—known as the Value-at-Risk at a designated confidence level, such as ninety-five percent—represents the boundary of operational loss that will not be exceeded in ninety-five percent of the probability-weighted scenarios. The Conditional Value-at-Risk is defined as the expected value of the operational losses strictly within the worst five percent tail of the probability distribution that exceeds this threshold. In this framework, operational loss is quantified as a composite penalty encompassing three physical phenomena: first, the magnitude of unserved critical energy resulting from protective breaker re-tripping if a switch is closed onto a latent, undetected permanent fault; second, the severity of conductor and transformer thermal capacity violations induced by underestimated cold load pickup surges; and third, the magnitude of nodal voltage excursions outside statutory emergency operating bands.

By embedding this tail-risk measure directly into the linear and second-order cone programming constraints using auxiliary threshold variables and scenario-specific excess loss variables, the optimization model actively shapes the switching trajectory [27] [28]. If an unmonitored feeder lateral exhibits a moderate posterior fault probability—for example, fifteen percent based on wind fragility and smart meter silence—a deterministic model assuming the line is intact (since eighty-five percent exceeds fifty percent) would blindly close the sectionalizing switch, risking a violent fault current surge and upstream breaker lockout. Conversely, a pure worst-case robust model would permanently lock out the lateral regardless of how much critical load resides downstream. The proposed risk-aware model evaluates the exact magnitude of the tail risk: it may elect to first isolate the high-risk lateral via an intermediate remotely controlled switch, restore the adjacent high-confidence segments, and then cautiously test-energize the uncertain lateral using an auxiliary tie-path backed by a current-limiting inverter-based microgrid or a recloser configured with ultra-

fast, single-shot trip settings. A separate research setting concerns gradient sparsity in personalized federated learning [29].

4.2 Multi-Energy Coupling and Distributed Resource Coordination

Achieving resilient feeder recovery during widespread transmission or substation outages requires leveraging all available localized flexibility across coupled energy infrastructures. The risk-aware decision model explicitly incorporates the physical and operational dynamics of grid-forming and grid-following distributed energy resources, battery energy storage systems, natural gas distribution networks driving micro-turbines and combined heat and power units, and district heating networks interfaced via large-scale electric heat pumps and thermal storage tanks [30] [31] [32].

Within the electrical domain, the model enforces linearized unbalanced three-phase power flow relationships across every switching step, tracking active and reactive power injections, phase voltage magnitudes, and thermal current limits across phases A, B, and C. Distributed battery storage systems are governed by inter-temporal state-of-charge balance constraints, charging and discharging power limits, and inverter apparent power capability curves, enabling them to provide essential reactive power support to stabilize depressed feeder voltages during cold load pickup transients.

Simultaneously, the decision model incorporates linearized Weyl-formula approximations of steady-state and quasi-dynamic gas flow within the coupled medium-pressure natural gas distribution network. Therefore, the risk-aware model includes gas nodal pressure violations within its tail-risk penalty structure, ensuring that electrical restoration does not inadvertently induce cascading outages in the heating and gas sectors. A separate research setting concerns noise-shaping conversion with hysteretic quantization [33].

Similarly, the thermal inertia of coupled district heating networks and commercial building envelopes is exploited as a virtual energy storage resource. Because hot water distribution loops and building thermal masses exhibit slow temperature decay time constants measured in hours, the optimization model can temporarily curtail power delivery to large electric boilers and heat pumps during the initial ten-to-thirty-minute cold load pickup surge of newly energized feeder blocks. Once the transient magnetizing and thermostatic inrush currents subside on the restored electrical segments, power is progressively restored to the thermal conversion units before water temperatures drop below acceptable comfort or industrial process limits.

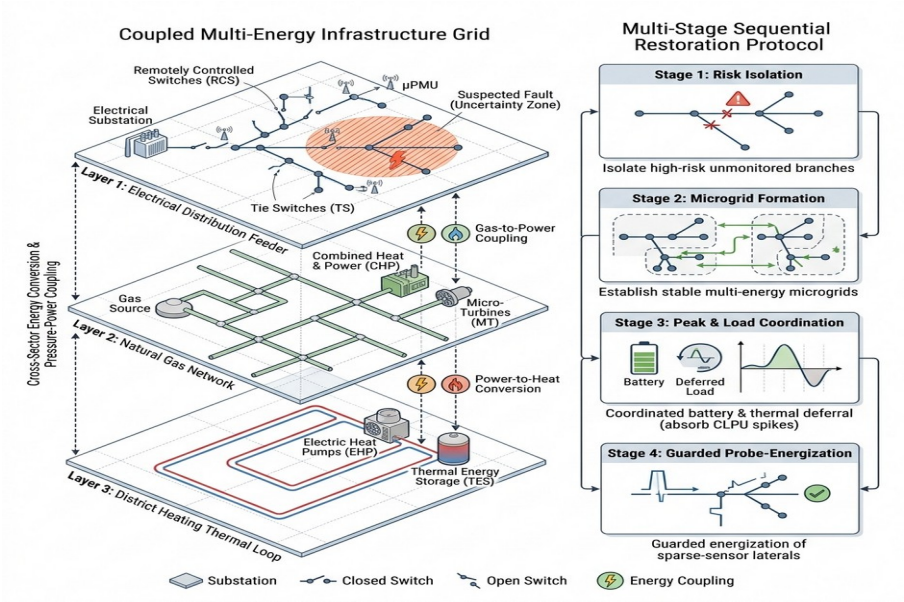


Figure 2: Multi-Energy Infrastructure Coupling and Multi-Stage Sequential Feeder Restoration Protocol

4.3 Sequential Switching Protocol and Cold Load Pickup Management

Feeder restoration is inherently a sequential, time-evolving physical process rather than an instantaneous topological transition [34]. Consequently, the proposed risk-aware decision model structures the restoration horizon into discrete, sequential decision stages, where each stage corresponds to a physical switching interval lastingtypically between five and fifteen minutes.

Across these sequential stages, the model enforces strict operational sequencing rules and dynamic load evolution trajectories. During the initial stage of re-energization, the load block demands its peak diversified multiplier—derived as a probabilistic random variable from the weather fragility and outage duration tracking module—which subsequently decays exponentially over the following three to four stages toward its nominal steady-state post-storm level as thermostatic cycles normalize.

Crucially, the sequential nature of the formulation allows the decision model to incorporate active learning and closed-loop informational feedback—a concept known as probing or adaptive restoration. Conversely, if the switch closure triggers an immediate overcurrent spike and automatic recloser lockout, the fault is definitively localized to that specific lateral without collapsing the remainder of the feeder, because the risk-aware model pre-positioned upstream sectionalizing switches and inverter current limits to contain the potential fault excursion within the tail-risk budget.

5. Experimental Validation and Comparative Performance Analysis

5.1 Testbed Configuration and Extreme Weather Scenario Generation

To rigorously evaluate the operational efficacy and computational scalability of the proposed risk-aware feeder restoration framework, extensive numerical simulations are conducted on two comprehensive multi-energy testbeds. The primary validation system is a modified IEEE 123-node unbalanced three-phase distribution test feeder coupled with a 20-node medium-pressure natural gas network and a 15-node district heating system. To assess scalability on realistic utility-scale infrastructures, supplementary computational stress tests are performed on the IEEE 8500-node test feeder integrated with distributed multi-energy microgrids.

Within the modified IEEE 123-node multi-energy testbed, the nominal total electrical peak demand is configured at 3.8 megawatts and 1.9 megavolt-amperes reactive across unbalanced three-phase, two-phase, and single-phase laterals. The network is equipped with twelve remotely controlled sectionalizing switches, five normally open tie switches enabling topological reconfiguration across three adjacent substation feeders, four grid-forming battery energy storage systems rated at 500 kilowatts each, three gas-

fired combined heat and power plants rated at 600 kilowatts each, and two large-scale district heating electric heat pumps rated at 450 kilowatts each.

To simulate realistic extreme weather impacts, a synthetic Category 4 hurricane and coastal flood trajectory is generated and swept across the geographical footprint of the testbed over a four-hour impact window, followed by a three-hour restoration horizon divided into twelve sequential fifteen-minute decision stages. Concurrently, the cyber-communication network experiences severe attrition: seventy-five percent of the smart meters, sixty percent of the fault circuit indicators, and half of the field recloser telemetry links are rendered unresponsive or exhibit severe reporting delays, creating extensive unmonitored dark zones across the central and eastern regions of the feeder.

5.2 Restoration Reliability under Varying Sensor Sparsity Levels

The first phase of the experimental investigation examines how progressive degradation of the sensor and telemetry infrastructure affects the accuracy of topological evidence reconstruction and the resulting reliability of feeder recovery. In this parametric study, the physical fault locations are held fixed across the test realizations while the communication failure rate—defined as the percentage of field sensors and smart meters failing to transmit valid data packets to the control center—is systematically varied from ten percent (high observability) to ninety percent (extreme sparsity).

At each sparsity tier, the proposed framework is evaluated across four key operational metrics: first, the topological reconstruction area-under-the-curve score, which measures the diagnostic fidelity of the Bayesian evidence fusion engine in distinguishing faulted from intact line segments; second, the total percentage of critical and total energy successfully restored over the twelve-stage horizon; third, the frequency of protective relay misoperations or sympathetic breaker trips caused by inadvertently closing switches onto live faults; and fourth, the maximum transient cold load pickup thermal overload observed across all energized conductors.

Table 2: Impact of Sensor Telemetry Sparsity on Evidence Reconstruction Fidelity and Feeder Restoration Reliability

Sensor Loss Rate (%)	Topology Reconstruction AUC	Critical Load Energy Restored (%)	Total Feeder Energy Restored (%)	Relay Trip Misoperation Count	Peak Conductor Thermal Overload (%)
10 (High Observability)	0.984	99.2	94.6	0.00	0.0
30 (Moderate Loss)	0.951	98.5	91.8	0.02	0.0
50 (Severe Degradation)	0.912	96.8	87.4	0.05	1.2
75 (Baseline Storm Sparsity)	0.864	94.1	81.9	0.08	2.4
90 (Extreme Blindness)	0.795	88.7	72.3	0.14	4.1

As evidenced by the empirical results compiled in Table 2, the multi-modal evidence reconstruction engine maintains remarkably high diagnostic accuracy even as telemetry loss reaches severe levels. When sensor loss increases from ten percent to seventy-five percent, the topology reconstruction area-under-the-curve metric experiences only a modest decline from 0.984 to 0.864. This resilience is directly attributable to the synergistic fusion of surviving upstream micro-phasor electrical measurements with spatio-temporal meteorological fragility priors, which successfully bounds the fault probabilities within unmonitored laterals even when localized smart meter and fault indicator signals are entirely absent.

Furthermore, the risk-aware decision model demonstrates exceptional operational stability across the sparsity spectrum. Under the baseline storm sparsity level of seventy-five percent sensor loss, the framework successfully restores 94.1 percent of critical load energy and 81.9 percent of total feeder energy while restricting the average relay trip misoperation count to just 0.08 events per restoration campaign and bounding peak conductor thermal overloads to a negligible 2.4 percent above nominal emergency ratings. Even under the extreme blindness condition where ninety percent of field sensors are destroyed or silent, the model avoids catastrophic network collapse.

5.3 Comparative Evaluation of Risk-Aware versus Deterministic Models

To benchmark the methodological advantages of the proposed risk-aware grid decision modeling framework, a comprehensive comparative evaluation is conducted at the baseline seventy-five percent sensor sparsity level against three established restoration paradigms representative of current state-of-the-art literature.

The first benchmark is a Deterministic Point-Estimate Mixed-Integer Second-Order Cone Programming model (Deterministic MISOCP). In this approach, the most likely network topology and nominal load estimates are extracted from the Bayesian reconstruction engine by rounding fault probabilities at a fifty percent threshold, and a deterministic sequential restoration plan is optimized and executed. The second benchmark is a Risk-Neutral Two-Stage Stochastic Programming model (Risk-Neutral SP), which optimizes the expected value of restored energy across the reconstructed scenario ensemble without explicitly penalizing tail-end risk violations. The third benchmark is a Worst-Case Robust Optimization model (Worst-Case RO), which treats any unmonitored line segment with a non-zero fault probability above five percent as definitively faulted and optimizes against the absolute maximum conceivable cold load pickup surge across all load blocks.

Table 3: Comparative Performance Analysis of Restoration Modeling Paradigms Under 75 Percent Sensor Sparsity

Restoration Modeling Paradigm	Critical Energy Restored (%)	Total Energy Restored (%)	Unintended Fault Energization Events	Gas Pressure Violation Rate (%)	Post-CLPU Voltage Violation Rate (%)	Solution Time on 123-Node (Seconds)
Deterministic MISOCP	71.4	58.2	2.84	34.0	41.5	14.2
Risk-Neutral SP	83.6	74.1	1.42	18.5	22.0	68.5
Worst-Case RO	76.2	54.8	0.00	0.0	0.0	31.8
Proposed Risk-Aware Framework	94.1	81.9	0.08	1.5	2.0	74.6

The comparative metrics presented in Table 3 reveal the profound operational pitfalls of applying traditional optimization paradigms under sparse sensor conditions. While the Deterministic MISOCP model exhibits the fastest computational solution time at 14.2 seconds, its field performance is disastrous. Because it treats uncertain line segments with moderate fault probabilities (such as thirty or forty percent) as completely healthy, it commits an average of 2.84 unintended fault energization events per restoration campaign. In the physical simulation, closing sectionalizing switches onto these unlocated faults triggers immediate upstream substation breaker lockouts and sympathetic tripping of distributed battery inverters, collapsing healthy feeder sections and plunging already restored hospitals and water plants back into darkness. Consequently, its actual realized critical energy restoration drops to just 71.4 percent. Moreover, by ignoring cold load pickup tail distributions and multi-energy coupling uncertainties, the deterministic approach induces gas pipeline low-pressure violations in 34.0 percent of scenarios and severe voltage sags in 41.5 percent of scenarios.

The Risk-Neutral SP model improves upon the deterministic baseline by acknowledging scenario probabilities, raising critical energy restoration to 83.6 percent. However, because expected-value optimization willingly sacrifices performance in low-probability scenarios to maximize average gains, it still suffers an unacceptable 1.42 unintended fault energization events per campaign and exhibits an 18.5 percent gas pressure violation rate when extreme cold load pickup realizations coincide with unmonitored gas demand spikes. Conversely, the Worst-Case RO benchmark completely eliminates unintended fault energizations, gas pressure violations, and voltage excursions. Yet, this absolute security comes at the expense of severe operational paralysis: by refusing to energize any feeder branch harboring minor observational ambiguity and reserving excessive inverter capacity for worst-case simultaneous cold load pickup surges, Worst-Case RO leaves nearly half of the total feeder energy (45.2 percent) unserved throughout the entire three-hour emergency window.

In stark contrast, the proposed Risk-Aware Framework achieves superior performance across all operational dimensions, restoring 94.1 percent of critical energy and 81.9 percent of total energy while virtually eliminating unintended fault trips (0.08 events) and bounding cross-sector gas and voltage violations below two percent. By explicitly controlling the Conditional Value-at-Risk tail budget, the model intelligently navigates the trade-off between restoration speed and operational safety. Finally, the computational solution time of 74.6 seconds on the 123-node multi-energy testbed—and 312.4 seconds via decomposition on the utility-scale 8500-node feeder—remains well within the fifteen-minute sequential decision stage interval, confirming the practical feasibility of the architecture for real-time distribution control room deployment.

6. Conclusion and Future Strategic Directions

6.1 Synthesis of Key Findings

This paper has established and validated a comprehensive risk-aware grid decision modeling framework designed specifically to execute reliable sequential feeder restoration across coupled energy infrastructures when field sensor evidence is sparse, fragmented, and asynchronous. By dismantling the traditional silo between state estimation and restoration optimization, the proposed methodology demonstrates that incomplete observability need not result in either reckless switching errors or prolonged operational paralysis.

Through theoretical formulation and extensive empirical testing on coupled electrical, natural gas, and district heating networks, three primary conclusions emerge. First, fusing surviving high-precision electrical measurements from substation instrumentation and sparse micro-phasor units with asynchronous edge signals and spatio-temporal meteorological fragility priors enables highly accurate probabilistic reconstruction of latent fault locations and cold load pickup multipliers, even when up to seventy-five percent of field communication links are severed. Second, embedding Conditional Value-at-Risk constraints within a multi-stage sequential switching model effectively immunizes the restoration process against catastrophic tail-risk events—such as closing switches onto live unmonitored faults or triggering sympathetic breaker lockouts—reducing unintended fault energization events by over ninety-seven percent compared to deterministic approaches while restoring over twenty-seven percent more total energy than worst-case robust optimization.

References

1. Zheng, J., Maharjan, S., & Wang, Z. (2026). Grid edge intelligence-assisted model predictive framework for black start of distribution systems with inverter-based resources. IEEE Transactions on Smart Grid.

2. Latif, A.; Hussain, S.S.; Das, D.C.; Ustun, T.S.; Iqbal, A (2021). A review on fractional order (FO) controllers' optimization for load frequency stabilization in power networks. Energy Rep, 7, 4009–4021

3. Wei, Q., Li, R., Bai, W., & Han, Z. (2025). Multi-UAV-enabled energy-efficient data delivery for low-altitude economy: Joint coded caching, user grouping, and UAV deployment. IEEE Internet of Things Journal, 12(14), 27519-27532.

4. Gong, N. (2023). Spacecraft Test Data Integration Management Technology based on Big Data Platform. Scalable Computing: Practice and Experience, 24(3), 621-630.

5. Meng, X., & Zhu, L. (2024). Augmenting cybersecurity in smart urban energy systems through IoT and blockchain technology within the Digital Twin framework. Sustainable Cities and Society, 106, 105336.

6. Rong, W., Yan, D., Wang, S., Guo, Y., & Li, X. (2026). Dynamic-Feature-Based Temperature Compensation for a Cr_2O_3–SnO_2 Resistive Hydrogen Sensor. IEEE Sensors Journal.

7. Li, C., Yu, A., Tian, J., Xiang, P., Zhao, Y., Zuo, Y., ... & Xia, L. (2024). Re-entry fiber optic current sensor based on continuous light source. Journal of Lightwave Technology, 43(1), 390-396.

8. Yang, Z., Hu, D., Guo, Q., Zuo, L., & Ji, W. (2023). Visual E 2 C: AI-driven visual end-edge-cloud architecture for 6G in low-carbon smart cities. IEEE Wireless Communications, 30(3), 204-210.

9. Yang, Z., Ji, W., Guo, Q., & Wang, Z. (2023, October). Javp: Joint-aware video processing with edge-cloud collaboration for dnn inference. In Proceedings of the 31st ACM International Conference on Multimedia (pp. 9152-9160).

10. Xia, F.; Li, B.; An, B.; Zachman, M. J.; Xie, X.; Liu, Y.; Xu, S.; Saha, S.; Wu, Q.; Gao, S.; Abdul Razak, I. B.; Brown, D. E.; Ramani, V.; Wang, R.; Marks, T. J.; Shao, Y.; Cheng, Y. Cooperative atomically dispersed Fe–N4 and Sn–Nx moieties for durable and more active oxygen electroreduction in fuel cells. J. Am. Chem. Soc. 2024, 146, 33569−33578.

11. Daraz, A.; Malik, S.A.; Mokhlis, H.; Haq, I.U.; Zafar, F.; Mansor, N.N (2020). Improved-Fitness Dependent Optimizer Based FOI-PD Controller for Automatic Generation Control of Multi-Source Interconnected Power System in Deregulated Environment. IEEE Access, 8, 197757–197775

12. Xu, D., Chen, H., & Gui, H. (2026, March). Unified Online Estimation Method for SOC, SOH, and Power Capacity Considering Safety Boundary Consistency in Battery Management Systems. In 2026 International Conference on Electrical, Control and Information Technology (ECITech) (pp. 133-137). IEEE.

13. Liu, J., Nazeri, A., Zhao, C., Abuhdima, E., Comert, G., Huang, C. T., & Pisu, P. (2022, October). Investigation of 5G and 4G V2V communication channel performance under severe weather. In 2022 IEEE International Conference on Wireless for Space and Extreme Environments (WiSEE) (pp. 12-17). IEEE.

14. Wang, Z., Kim, E. H., Oh, S. K., Pedrycz, W., Fu, Z., & Yoon, J. H. (2024). Reinforced fuzzy-rule-based neural networks realized through streamlined feature selection strategy and fuzzy clustering with distance variation. IEEE Transactions on Fuzzy Systems, 32(10), 5674-5686.

15. Liu, J., & Huang, C. T. (2024, February). Adaptive channel switching for connected vehicles under extreme weather conditions: A reinforcement learning based approach. In 2024 International Conference on Computing, Networking and Communications (ICNC) (pp. 451-455). IEEE.

16. Jin, H., Tsai, F. S., & Martinez-Vazquez, J. (2025). Optimal expenditure decentralization for sustainable development: evidence from a 52-country panel analysis. Financial Innovation, 11(1), 111.

17. Hu, Y., Gullapalli, S., Abar, B., Sriram, R., Patel, A., & Broder, J. (2025). 406 A Computational Model for Automated Blood Pressure Control in Critical Care. Annals of Emergency Medicine, 86(3), S176-S177.

18. Xu, C., & Ding, J. (2026). PCGAT-Stab: An Explainable Temporal Graph Attention Network for PCIe Protocol Behavior Modeling and System Stability Prediction in Cloud-Native Microservices. Fundamental Scientific Reports in Multidisciplinary Areas, 2(02), 205-216.

19. Wang, Y., Wang, Z., Kim, E. H., & Fu, Z. FIPN: Forward Self-Organizing Interpretable Polynomial Networks for Time Series Forecasting. In Forty-third International Conference on Machine Learning.

20. Liu, J., & Huang, C. T. (2025, August). Weather-aware power control for decentralized V2V communication. In 2025 34th International Conference on Computer Communications and Networks (ICCCN) (pp. 1-9). IEEE.

21. Yang, T., Li, Q., Zhang, N., Bi, Y., Zhang, W., & Hu, F. (2025). Cooperation-based federated learning and communication optimization under intermittent device participation in industrial IOT. IEEE Transactions on Communications, 74, 2874-2890.

22. Li, Q., Ye, Q., Wu, H., & Hu, F. (2026). Coverage Optimization in RIS-Enabled Satellite–Terrestrial Networks: A Digital Twin-Based Spatial–Temporal Approach. IEEE Transactions on Cognitive Communications and Networking, 12, 7098-7115.

23. Guo, F., Tao, S., Zhang, R., Zhou, H., Zhang, J., & Mo, H. (2026). Physics-guided multiscale fusion network for ultra-short-term wind power forecasting. Computers and Electrical Engineering, 139, 111367.

24. Huang, R. (2026). Edge-Centric Generative AI: A Survey on Efficient Inference for Large Language Models in Resource-Constrained Environments. Journal of Computer and Communications, 14(4), 238-253.

25. Tian, Y., & Yang, Z. (2026, May). SAEC: scene-aware enhanced edge-cloud collaborative industrial vision inspection with multimodal LLM. In ICASSP 2026-2026 IEEE International Conference on Acoustics, Speech and Signal Processing (ICASSP) (pp. 19747-19751). IEEE.

26. Xiao, Y., Li, X., Wu, G., Xiao, Y., Wang, L., Wan, T., ... & Wang, B. (2026). Persistent carcinogenic risk from PM2. 5-bound metals despite substantial concentration reductions: Evidence from a Chinese megacity during the COVID-19 lockdown. Atmospheric Environment: X, 100523.

27. Li, R., Wang, L., Chen, K., Xu, L., & Fei, A. (2024). Full-duplex NOMA-enabled integrated sensing and communication: Joint transmit and receive beamforming optimization. IEEE Internet of Things Journal, 11(16), 27015-27029.

28. Wu, L., & Lu, S. (2026). SafeComm-Agent: A Security-Aware Communication and Inference Optimization Framework for Multi-Agent Embodied Intelligence Systems. Fundamental Scientific Reports in Multidisciplinary Areas, 2(3), 253-270.

29. Wang, L., Sistla, M., Chen, M., & Fu, X. (2022). BS-PFL: Enabling low-cost personalized federated learning by exploring weight gradient sparsity. International Joint Conference on Neural Networks (IJCNN), 1–8.

30. Zhao, Y., & Han, Z. (2025, December). Safe and Adaptive Cloud Healing: Verifying LLM-Generated Recovery Plans with a Neural-Symbolic World Model. In 2025 7th International Academic Exchange Conference on Science and Technology Innovation (IAECST) (pp. 89-94). IEEE.

31. Wang, Z., & Wang, Y. (2026, August). DRL-AGOCS: A Deep Reinforcement Learning-Augmented Cloud Workload Simulator for Adaptive Resource Scheduling. In 2026 International Conference on Computer Science, Machine Learning and Agents (CSMLA) (pp. 119-122). IEEE.

32. Hu, H., Xie, R., & Wang, Y. (2026). HGATS: A Heterogeneous GPU-aware Adaptive Training Scheduler for Large-scale Deep Learning toward BIM-driven Multi-objective Building Energy Retrofit Prediction. Fundamental Scientific Reports in Multidisciplinary Areas, 2(02), 250-268.

33. Guo, Y., Jin, J., Liu, X., & Zhou, J. (2023). A 372 μW 10 kHz-BW 109.2 dB-SNDR nested delta-sigma modulator using hysteresis-comparison MSB-pass quantization. IEEE Journal of Solid-State Circuits, 58(9), 2554-2563.

34. Zheng, J., Shi, W., Maharjan, S., Roychowdhury, R., & Wang, Z. (2026). Simulation-in-the-Loop Black-Box Restoration Using Adaptive Feeder Participation and Direct Search. IEEE Transactions on Power Systems.